ATOMIC CALCULATION FOR THE ATMOSPHERES OF STRONGLY-MAGNETIZED NEUTRON STARS

KAYA MORI AND CHARLES J. HAILEY Columbia Astrophysics Laboratory, New York, NY 10027 Accepted for publication in the Astrophysical Journal

ABSTRACT

Complete modeling of radiative transfer in neutron star atmospheres is in progress, taking into account the anisotropy induced by magnetic fields, non-ideal effects and general relativity. As part of our modeling, we present a novel atomic calculation method producing an extensive atomic data set including energy values and oscillator strengths in the so-called Landau regime $(B > 4.7 \times 10^9 Z^2 \text{ G})$. Conventional atmosphere models for B = 0 are not applicable to typical field strengths of cooling neutron stars $(B \sim 10^{12} - 10^{13} \text{ G})$, since an atom no longer keeps its spherical shape. The elemental composition and the configuration of the magnetic field in the atmosphere are presently unknown, so that atomic data must be produced for ground and excited states of several ions as a function of magnetic field. To accomplish this efficiently, we minimized the iterations in the Hartree equation and treated exchange terms and higher Landau states by perturbation methods. This method has the effect of reducing the computation time significantly. Inclusion of higher Landau states gives us much more accurate data for inner orbitals unlike other methods based on the adiabatic approximation. While existing atomic data in the Landau regime are available only for low Z atoms, our method can be used in elements up to Fe with sufficient accuracy to be of use for spectroscopic missions such as Chandra, Chandra,

Subject headings: atomic processes — magnetic fields — stars: neutron

1. INTRODUCTION

Since their discovery in 1967 (Hewish et al. 1968), pulsars have attracted the interest of researchers in various fields due to their exotic properties and extreme physical conditions. Although many of the pulsars were discovered in the radio band, multi-wavelength studies have helped to elucidate their properties. ROSAT discovered thermal components ($T \sim 10^5 - 10^6$ K) from the so-called cooling neutron stars in the soft X-ray band (Becker & Trümper 1997). Emergent spectra from the photosphere can be modified from a pure blackbody spectrum by the presence of an atmosphere (Romani 1987). The geometrical thickness of neutron star atmospheres is small ($\sim 0.1 - 100$ cm) due to the strong gravitational field (Pavlov et al. 1995). Nevertheless, it can be optically thick for reprocessing thermal photons due to the high density.

With great improvements in the sensitivity and the resolution of recent X-ray telescopes, X-ray spectroscopy can directly provide information on the surface of neutron stars. There are two possible implications that the atmosphere may have on the X-ray spectrum. Precise measurement of surface temperature taking into account the atmospheric effects is crucial for determining the cooling curves of neutron stars, which constrains various equations of state (Tsuruta 1995; Page 1998; Yakovlev et al. 1999). Secondly, atomic (line or edge) absorption features along with cyclotron lines enable us to diagnose properties of the atmosphere.

Magnetic field (B) can be measured directly by the observation of cyclotron lines (Trümper et al. 1978; Wheaton et al. 1979), or indirectly by the spindown rate of pulsars assuming a dipole magnetic configuration (Ostriker & Gunn 1969). Most of the observed pulsars are believed to

possess very strong magnetic fields ($B \sim 10^{11} - 10^{13} \text{ G}$). except the millisecond pulsars whose magnetic fields are relatively low $(B \sim 10^{8} - 10^{10} \text{ G})$ (Camilo et al. 1994). Surface elements (Z) are not known at present. Strong gravity stratifies the surface layers so that the lightest element resides at the top of the atmosphere (Alcock & Illarionov 1980). However, any element between H and Fe is feasible. Accretion from the interstellar medium could accumulate a hydrogen layer, while an Fe atmosphere is favored from the study of the mass-cut in supernova explosions (Woosley & Weaver 1986). Lighter elements are formed by the spallation of heavy nuclei by particles (Miller 1990). On the other hand, pycnonuclear reactions could produce heavier nuclei from light nuclei (Lai & Salpeter 1997; Salpeter 1998). The fallback from the outer shells of supernova remnants could be of any element (Chevalier 1996). The surface density (ρ) is also uncertain in the range of $\rho \sim 0.1-10~{\rm gcm^{-3}}$ (Pavlov et al. 1995). The state of matter on the surface could be liquid, solid or in the form of molecular chains along the field (Abrahams & Shapiro 1991; Lai et al. 1992; Demeur et al. 1994; Ortiz et al. 1995; Lai & Salpeter 1996, 1997). In high density plasma, atoms are strongly-coupled, inducing nonideal effects, and electrons may be partially degenerate.

2. Atmosphere models

There have been several attempts at modeling magnetized neutron star atmospheres. For weakly-magnetized pulsars ($B \leq 10^9$ G), atmosphere models for B=0 are applicable (Romani 1987; Rajagopal & Romani 1996; Zavlin et al. 1996). These non-magnetic atmosphere models have been applied to several neutron stars (Zavlin & Pavlov 1998; Pons et al. 2000). However, for the strongly-magnetized atmospheres ($B > 10^9$ G), atomic models re-

quire a new scheme quite different from the conventional atomic calculations for the B = 0 case. For instance, the ionization threshold of a hydrogen atom increases to 160 eV at $B=10^{12}$ G. Also, in the presence of a strong magnetic field photon opacities are highly dependent on the direction of the magnetic field and the polarization of photons (Pavlov et al. 1995). Thermodynamic properties of hydrogen atmospheres have been intensively investigated by Lai & Salpeter (1995), Steinberg et al. (1998) and Potekhin et al. (1999). They have computed the equation of state and the degree of ionization assuming LTE and taking into account coupling effects such as the motional Stark field and the pressure ionization peculiar to a strongly-magnetized dense plasma. The hydrogen atmosphere model of Potekhin et al. (1999) is constructed based on the accurate atomic database obtained by Potekhin (1998). Recently, Ozel (2001) and Ho & Lai (2001) studied spectral signatures from atmospheres of strongly magnetized neutron stars, utilizing improvements in radiative transfer theory. However, they assumed fully-ionized hydrogen atmospheres. Therefore their results are limited to rather high temperature. Similarly, Zane et al. (2000) studied fully-ionized hydrogen atmospheres of accreting neutron stars. Fully-ionized hydrogen atmosphere models have been applied to data on isolated neutron stars obtained by XMM-Newton and Chandra (Paerels et al. 2001; Pavlov et al. 2001). In contrast, radiative transfer in partially-ionized hydrogen atmosphere with full inclusion of bound-bound and bound-free opacities remains to be solved in comparison with recent X-ray data.

On the other hand, atmosphere models of high Z atoms are still immature due to their increased complexity. Miller (1992) was the first to construct model atmospheres for Z=2-7. However, the opacities include only bound-free cross sections with averaging of the polarization modes. Fe atmospheres were investigated by Rajagopal et al. (1997); the model is rather crude and the energy values and oscillator strengths have as much as 10% and a factor of two uncertainties, respectively. Both of the atmosphere models for Z>1 elements are based on atomic calculation by the Hartree-Fock method of Neuhauser et al. (1987).

As the spectroscopy capability of X-ray telescopes improves, model atmospheres of strongly-magnetized neutron stars should comparably improve. Our efforts are focused on constructing atmosphere models for Z>1 atoms for comparison with existing hydrogen atmosphere models and new X-ray observations. As part of this effort, we present a novel atomic calculation appropriate for model atmospheres of strongly-magnetized neutron stars. A brief review of atomic structure in strong magnetic fields is given in $\S 3$, then various atomic calculations are described in $\S 4$ in comparison with our formalism in $\S 5$. Subsequently, the validity of our model and relevant physical processes are discussed in $\S 6$. Some numerical improvements are mentioned in $\S 7$. Finally, we present our results in comparison with previous atomic models in $\S 8$.

3. ATOMIC STRUCTURE IN STRONG MAGNETIC FIELD

When a strong magnetic field is present, the spherical symmetry of an atom is broken and the atom is stretched along the field. The Landau regime is defined as that where the magnetic field effects exceed Coulomb field effects, i.e. $\hbar\omega_B>Ze^2/r$ ($\hbar\omega_B=11.57B_{12}$ keV = electron cyclotron energy, $B=10^{12}B_{12}$ G). This is translated to $\beta_Z\geq 1$, where $\beta_Z=B/Z^2B_0$, $\beta=B/B_0$ and the reference field $B_0=4.701\times 10^9$ G, as a good measure for the relative strength of magnetic field to the nuclear Coulomb field. The dominance of the magnetic field requires us to investigate the atomic structure exploiting cylindrical symmetry. In cylindrical coordinates (ρ,ϕ,z) bound electrons in an atom are well described by the four quantum numbers (n,m,ν,s_z) denoting Landau number, magnetic quantum number, longitudinal quantum number and component of electron spin along the field respectively. ν is the node of the longitudinal wavefunction and it defines the parity along the field as $(-1)^{\nu}$. $\nu=0$ states are located close to the nucleus (tightly-bound orbitals), while $\nu>0$ states are far from the nucleus (loosely-bound orbitals).

In very strong magnetic fields $(\beta_Z \gg 1)$ it is a fairly good approximation to fix n=0 (adiabatic approximation) and $m \leq 0, s_z = -1/2$ (full-spin-polarization, FSP hereafter). Various atomic models have adopted both assumptions (i.e. restrict the two quantum numbers n and s_z) because they simplify calculations. Accordingly, bound electrons are characterized by a set of two quantum numbers (m, ν) (m indicates its absolute value, hereafter). However, as β_Z approaches 1 the occupation in n > 0 Landau levels is not negligible (configuration mixing), so the adiabatic approximation does not provide accurate atomic data (Jones et al. 1999b). With further decrease in the magnetic field, spin-flip transitions take place, i.e. the FSP structure is no longer a ground state since an electron with the opposite spin lowers the total energy (Ivanov & Schmelcher 2000).

The intermediate field regime is defined as that at which the electric field and magnetic field becomes comparable. Bound electrons feel differing electric fields depending on their distance from the nucleus and the screening of nuclear charge by inner electrons. A critical field strength B_c which defines the intermediate regime is determined by equating the Coulomb force and the Lorentz force. Assuming that the distance of the (m,0) orbital to the nucleus is $\sim (2m+1)^{1/2}\hat{\rho}$ where $\hat{\rho}$ is the cyclotron radius $\hat{\rho}=2.566\times 10^{-10}B_{12}^{-1/2}$ cm and Z_{eff} is the effective charge, B_c is given by (Miller 1990),

$$B_c = \frac{Z_{eff}^2}{2(2m+1)^3} B_0. (1)$$

A choice of either pure spherical or cylindrical basis functions is not sufficient for accurate atomic structure calculations in the intermediate field regime. Nonseparability of ρ and z in the nuclear Coulomb term prevents an analytical solution of the Schrödinger equation even for hydrogenic atoms. For Z>1 atoms, electron-electron interactions add more complication to the problem.

4. ATOMIC CALCULATIONS IN THE LANDAU REGIME

Various atomic models have been proposed in the Landau regime. First of all no experimental data is available at high magnetic fields $B>10^7$ G. Therefore atomic data are highly model-dependent. Hydrogen has been investigated by various authors for the last 20 years (see Ruder et al. (1994), Lai (2000) and references therein). Very accurate

energy values and oscillator strengths were obtained at arbitrary field strength with full inclusion of various effects such as relativistic correction (Chen & Goldman 1992) and motional Stark effect (Potekhin 1998).

For Z>1 atoms, the number of studies is significantly smaller. Atomic calculations for multi-electron atoms are often classified as ab initio or self-consistent methods. Ab initio methods include the restricted variational method (Chen et al. 1974; Flowers et al. 1977; Glasser & Kaplan 1975; Glasser 1975; Müller 1984) and statistical methods. The restricted variational method parameterizes the wavefunctions in an ab initio way, so the accuracy usually remains poor compared with other methods. Statistical approaches such as the Thomas-Fermi method (TF hereafter) or Thomas-Fermi-Dirac method (TFD hereafter) (Skjervold & Ostgaard 1984; Lieb et al. 1992; Rögnvaldsson et al. 1993; Thorolfsson et al. 1998) are applicable to an atom with many electrons, usually for Z>10.

In general self-consistent methods are more accurate than ab initio methods, but they are computationally intensive since they entail iterative calculations. The one-dimensional Hartree-Fock method of Neuhauser et al. (1987) (1DHF hereafter) was the first self-consistent method for multi-electron atoms in the Landau regime. Since the adiabatic approximation is assumed in their calculations, the Hartree-Fock equation reduces to a one-dimensional equation along the magnetic field. They provided energy values of ground states for Z=1-18 and 26. Miller & Neuhauser (1991) obtained energy values and oscillator strengths for $Z \leq 14$ based on Neuhauser's atomic code. As mentioned by Miller & Neuhauser (1991), the inclusion of n>0 Landau levels to the Hartree-Fock equation is extremely difficult.

In recent years several sophisticated atomic models were proposed and studied for low Z atoms (Jones et al. 1999b; Ivanov & Schmelcher 1998, 1999, 2000). One of them is the two-dimensional Hartree-Fock method (2DHF hereafter), which unrestricted wavefunctions both in the transverse and longitudinal direction (Ivanov & Schmelcher 2000). It unrestricted the electron spin as well. Therefore, 2DHF is in principle applicable at any field strength, providing very accurate results through improved numerical accuracy. Jones et al. (1999b), who also adopted a similar unrestricted Hartree-Fock method with even-tempered gaussian basis functions (UHF hereafter), pointed out that the adiabatic approximation provides accurate atomic data only at $\beta_Z > 50$. Since typical magnetic fields of neutron stars can be at $\beta_Z < 50$ for high Z surface elements, energy values obtained by 1DHF could be severely inaccurate in the soft X-ray band where high energy resolution spectroscopy is now available. On the other hand, atomic data from 2DHF and UHF were computed only for energy levels of ground states and several low-lying states of low Z atoms ($Z \le 6$ for UHF, $Z \le 10$ for 2DHF) due to computation time limits. However, spectroscopy requires energy levels and oscillator strengths for various excited states as well.

The density-functional method (DF hereafter) was applied to multi-electron atoms in the Landau regime (Jones 1985a,b, 1986; Kössl et al. 1988; Relovsky & Ruder 1996; Johnsen & Yngvason 1996; Holas & March 1997). It pa-

rameterizes the relevant terms in the Hamiltonian (including the exchange term and electron correlation term) as a function of electron density in the Kohn-Sham equation. However, results are highly dependent on the choice of the exchange-correlation density functional (Jones 1985a). Neuhauser et al. (1987) mentioned that the density functionals of Jones (1985a, 1986) and Kössl et al. (1988) are not quite correct in high magnetic fields. In addition, DF becomes inaccurate for an atom with a few electrons.

Other atomic calculations with accuracy $\sim 10^{-4}$ such as the Quantum Monte-Carlo (QMC) method or the Configuration Interaction (CI) method have been proposed but have been implemented only for two-electron systems (Jones et al. 1997; Scrinzi 1998; Becken et al. 1999; Becken & Schmelcher 2000). CI method has been extended to high angular momentum states of helium (Becken & Schmelcher 2001). Nevertheless, it required 9 months of computing relevant matrix elements to produce an exhaustive atomic database. Recently, spectral features from the white dwarf GD229 have been successfully explained by helium in a magnetic field of few× 10^8 G (Jordan et al. 1998; Jones et al. 1999a).

Given the lack of experimental data, the self-consistent method is required to generate atomic data sufficiently accurate for refined X-ray spectroscopy. An extensive and accurate atomic data set for various atoms and ion states from Z=1 to 26 in the Landau regime is necessary for the X-ray spectroscopy of cooling neutron stars. This contrasts with recent work which has concentrated on low Z atoms spanning a wide range of magnetic field, achieved with 2DHF and UHF.

In the next section, after a brief description of our formalism, we describe our novel approach, which we call the multi-configurational, perturbative, hybrid, Hartree, Hartree-Fock method (MCPH³). The technique allows us to achieve an exhaustive list of energy values and oscillator strengths at various magnetic fields with very fast computation times on small computers.

5. FORMALISM

5.1. Schrödinger equation preliminaries

The non-relativistic Hamiltonian in a uniform magnetic field (assuming infinite nuclear mass) H is divided into a 0th order Hamiltonian $H^{(0)}$ and a perturbation $H^{(1)}$. We set the electron g-factor to 2.

$$H = \sum_{i} \left[\frac{1}{2m_{e}} \left(\vec{p_{i}} + \frac{e\vec{A}}{c} \right)^{2} + \frac{e}{m_{e}c} \vec{B} \cdot \vec{s_{i}} - \frac{Ze^{2}}{|\vec{r_{i}}|} \right]$$

$$+ \sum_{i} \sum_{j < i} \frac{e^{2}}{|\vec{r_{i}} - \vec{r_{j}}|}$$

$$= \sum_{i} \left[\frac{1}{2m_{e}} \left(\vec{p_{i}} + \frac{e\vec{A}}{c} \right)^{2} + \frac{e}{m_{e}c} \vec{B} \cdot \vec{s_{i}} + V_{nuc}(\vec{r_{i}}) \right]$$

$$+ V_{eff}(\vec{r_{i}}) \right] + \sum_{i} \left[\left(\sum_{j < i} \frac{e^{2}}{|\vec{r_{i}} - \vec{r_{j}}|} \right) - V_{eff}(\vec{r_{i}}) \right]$$

$$= H^{(0)} + H^{(1)}.$$

$$(2)$$

The vector potential of the uniform magnetic field $\vec{A} = \frac{1}{2}\vec{B}\times\vec{r}$ is chosen so that the magnetic field is along the z coordinate $\vec{B} = \nabla\times\vec{A} = B\hat{z}$. Hereafter, all the lengths are measured in units of $\hat{\rho}$. $V_{nuc}(\vec{r_i})$ is the nuclear Coulomb potential. $V_{eff}(\vec{r_i})$ is the effective potential for electron i and represents the mean Coulomb potential from the other electrons via the Hartree potential.

$$V_{eff}(\vec{r}_i) = \frac{e^2}{\hat{\rho}} \sum_{j \neq i} \int d^3 \vec{r}_j \, \frac{|\phi_{m_j \nu_j}(\vec{r}_j)|^2}{|\vec{r}_i - \vec{r}_j|}.$$
 (4)

 $H^{(0)}$ consists of single-orbital Hamiltonians :

$$H^{(0)} = \sum_{i} h_i^{(0)}. (5)$$

For an orbital (m, ν) (hereafter we omit the index i), the Schrödinger equation in the Hartree approximation becomes,

$$h^{(0)} \cdot \phi_{m\nu}(\vec{r}) = \epsilon_{m\nu}^{(0)} \cdot \phi_{m\nu}(\vec{r}). \tag{6}$$

5.2. Multiconfigurational, Perturbative, Hybrid, Hartree, Hartree-Fock: The Approach

Given the formalism above we can now outline the MCPH³ approach and describe its advantage. MCPH³ method starts with equation (6), which is the single-orbital Hartree equation for the unperturbed Hamiltonian $H^{(0)}$. We note that (1) $\beta_Z > 1$ and (2) the Hartree potential is orbital independent. The former implies the occupation of n > 0 Landau levels is small compared to the n = 0 state. Therefore equation (6) is amenable to a solution in which we break the singleorbital Hamiltonian $(h^{(0)})$ into a 0th order term $(\tilde{h}^{(0)})$ and a 1st order term $(\tilde{h}^{(1)})$. The $\tilde{h}^{(0)}$ term will represent a purely single-configurational calculation for the single-orbital wavefunction. The orbital-independence of the Hartree-potential will ensure that we can restrict the iterative calculation of the Hartree wavefunction to the n = 0 single-configurational (one dimensional) calculation; once we have determined the longitudinal part of this wavefunction $(f_{m\nu})$ iteratively, it will be immediately applicable to the construction of the multi-configurational Hartree single-orbital wavefunctions without further need for iterative calculations. This represents an enormous computational simplification over the schemes employed for hydrogen atoms (Rösner et al. 1984; Forster et al. 1984) in which the longitudinal wavefunction for each Landau level in the multi-configurational solution must be calculated separately.

With a set of eigenfunctions $(\chi_{nm\nu})$ for the 0th order single-configurational Hamiltonian $\tilde{h}^{(0)}$ determined we can solve for the multi-configurational single-orbital wavefunctions $(\phi_{m\nu})$ and energy eigenvalues $(\epsilon_{m\nu}^{(0)})$ using perturbation theory with $\tilde{h}^{(1)}$. We construct the total wavefunction $\Psi(\vec{r})$ for $H^{(0)}$ by forming a completely antisymmetrized spatial wavefunction from the $\phi_{m\nu}$ (as required by the FSP assumption). This total wavefunction $\Psi(\vec{r})$ can then be used along with $H^{(1)}$ of equation (3) to solve for the energy of the total Hamiltonian using simple 1st order perturbation theory.

This approach is, in effect, a double application of perturbation theory. In the first application perturbation theory is used on the single-orbital Hamiltonian to handle the higher Landau levels and solve for the multiconfigurational, single-orbital energies and wavefunctions (with only 1 iterative calculation required). In the second application 1st order perturbation theory on the total wavefunction and total Hamiltonian yields the total energy. This same wavefunction is used to calculate oscillator strengths. To avoid confusion we call the first application perturbation theory of type I and the second application perturbation theory of type II.

This is similar to the Z–expansion method in which the whole electron-electron interaction term is treated as a perturbation (Hylleraas 1930). However, the Z–expansion method is accurate only for highly ionized atoms. Our 0th order wavefunction is much more accurate for multi-electron atoms due to its self-consistency. As a result, we achieved fast convergence (3–5 iterations for less than 0.1% convergence in total energies) and numerical stability over all the electron configurations we have computed for Z=1-26 atoms. The method presented in this article is valid to $\beta_Z>1$, covering the typical magnetic fields of cooling neutron stars for the surface elements up to Fe (figure 1).

5.3. The MCPH³ solution for the multiconfigurational, single-orbital Hartree wavefunctions and energies (Type I perturbation theory)

The single-orbital Hamiltonian $h^{(0)}$ in (6) is divided into the 0th order and its perturbation as follows.

$$h^{(0)} = \tilde{h}^{(0)} + \tilde{h}^{(1)},\tag{7}$$

where

$$\tilde{h}^{(0)} = h_B(\rho, \phi) + h_L(z), \tag{8}$$

$$\tilde{h}^{(1)} = \{V_{nuc}(\vec{r}) - V_{nuc}(z)\} + \{V_{eff}(\vec{r}) - V_{eff}(z)\}. \tag{9}$$

 $h_B(\rho, \phi)$ is the transverse Hamiltonian, whose eigenvalue and eigenfunction are $n\hbar\omega_B$ and $\Phi_{nm}(\rho, \phi)$ (see below). Due to the separation of variables in $\tilde{h}^{(0)}$, eigenfunctions and eigenvalues of the Schrödinger equation for $\tilde{h}^{(0)}$:

$$\tilde{h}^{(0)} \cdot \chi_{nm\nu}(\vec{r}) = \epsilon_{nm\nu} \cdot \chi_{nm\nu}(\vec{r}) \tag{10}$$

are given by

$$\chi_{nm\nu}(\vec{r}) = \Phi_{nm}(\rho, \phi) \cdot f_{m\nu}(z), \tag{11}$$

$$\epsilon_{nm\nu} = n\hbar\omega_B + \epsilon_{0m\nu}.\tag{12}$$

 $\{\chi_{nm\nu}\}\$ is a complete set of orthogonal eigenfunctions of $\tilde{h}^{(0)}$. $\epsilon_{0m\nu}$ is an energy eigenvalue obtained by the single-configurational calculation for n=0 (see below). The transverse wavefunction $\Phi_{nm}(\rho,\phi)$ is a Landau function defined as (Landau & Lifshitz 1965),

$$\Phi_{nm}(\rho,\phi) = \frac{\sqrt{n!}}{\sqrt{2\pi(n+m)!}} \left(\frac{\rho}{\sqrt{2}}\right)^m e^{-\rho^2/4} \times L_n^m \left(\frac{\rho^2}{2}\right) e^{-im\phi}, \quad (13)$$

satisfying the orthonormal condition

$$\int \rho d\rho \int d\phi \,\, \Phi_{nm}^*(\rho,\phi) \cdot \Phi_{n'm'}(\rho,\phi) = \delta_{nn'}\delta_{mm'}. \tag{14}$$

5.3.1. Single-configurational calculation for n = 0

An equation for $h_L(z)$ can be found by multiplying the equation (6) by $\Phi_{0m}^*(\rho,\phi)$ and integrating over ρ and ϕ .

$$h_L(z) \cdot f_{m\nu}(z) = \epsilon_{0m\nu} \cdot f_{m\nu}(z), \tag{15}$$

where

$$h_L(z) = -\frac{\hbar^2}{2m_e\hat{\rho}^2} \frac{d^2}{dz^2} + V_{nuc}(z) + V_{eff}(z).$$
 (16)

The single-configurational nuclear and effective potentials are defined for n=0 as,

$$V_{nuc}(z) = \int \rho d\rho \int d\phi \ V_{nuc}(\rho, z) |\Phi_{0m}(\rho, \phi)|^2,$$

$$V_{eff}(z) = \int \rho d\rho \int d\phi \ V_{eff}(\rho, \phi, z) |\Phi_{0m}(\rho, \phi)|^2.$$
 (17)

We seek an eigenvalue $\epsilon_{0m\nu}$ with the node ν under the boundary condition $f_{m\nu}(z) \to 0$ at $z=\pm\infty$ with the solution for $f_{m\nu}(z)$. The only iterative part to the entire solution for H is complete with this calculation toward the convergence of $\epsilon_{0m\nu}$ and $f_{m\nu}(z)$; the one-dimensional effective potential $V_{eff}(z)$ is constructed from wavefunction of other orbitals and the equation (15) is solved for a new energy eigenvalue and longitudinal wavefunction.

5.3.2. Perturbation to higher Landau levels

With the eigenvalues and eigenfunctions of $\tilde{h}^{(0)}$ determined, we can proceed to obtain the multi-configurational, single-orbital wavefunction $\phi_{m\nu}(\vec{r})$ using perturbation theory. We expand $\phi_{m\nu}(\vec{r})$ as

$$\phi_{m\nu}(\vec{r}) = \sum_{n} c_{nm\nu} \cdot \chi_{nm\nu}(\vec{r}). \tag{18}$$

The coefficients $c_{nm\nu}$ are computed by the usual non-degenerate perturbation theory (as is the energy $\epsilon_{m\nu}^{(0)}$).

$$c_{nm\nu} = c_{nm\nu}^{(0)} + c_{nm\nu}^{(1)} + c_{nm\nu}^{(2)} + \dots$$
 (19)

Matrix elements of the 0th order Hamiltonian between different n but the same (m, ν) are simply $\langle nm\nu|\tilde{h}^{(0)}|n'm\nu\rangle = (n'-n)\hbar\omega_B$ where $\langle \vec{r}|nm\nu\rangle \equiv \chi_{nm\nu}(\vec{r})$. The matrix elements of $\tilde{h}^{(0)}$ become 0 for different m states due to the orthogonality of Landau functions. The perturbation terms between different ν states are also 0, because different ν states are orthogonal to each other. On the other hand, matrix elements of $\tilde{h}^{(1)}$ between different Landau states consist of two parts as follows.

$$\langle nm\nu | \tilde{h}^{(1)} | n'm\nu \rangle = \langle nm\nu | V_{nuc}(\vec{r}) | n'm\nu \rangle + \langle nm\nu | V_{eff}(\vec{r}) | n'm\nu \rangle.$$
 (20)

For the evaluation of the matrix elements, the reader should refer to the appendix.

5.4. The MCPH³ solution for the total wavefunction and energy of the Hamiltonian (Type II perturbation theory)

Once the Hartree single-orbital wavefunctions $\phi_{m\nu}(\vec{r})$ in (18) are orthonormalized, the 0th order total wavefunction is given as below since the spatial wavefunction must be antisymmetrized based on the FSP assumption.

$$\Psi(\vec{r}) = A \prod_{m} \phi_{m\nu}(\vec{r}), \tag{21}$$

where A is the antisymmetrizing operator.

Based on the total spatial wavefunction in (21), we evaluate the single-orbital energy (which is the ionization threshold) $\epsilon_{m\nu}$ and total energy E to the 1st order in perturbation theory (called type II perturbation theory in §5.2). The single-orbital energy is given by,

$$\epsilon_{m\nu} = \epsilon_{m\nu}^{(0)} + \epsilon_{m\nu}^{(1)},\tag{22}$$

where

$$\epsilon_{m\nu}^{(1)} = \langle \Psi | \left(\sum_{m'\nu'} \frac{e^2}{|\vec{r} - \vec{r}'|} - V_{eff}(\vec{r}) \right) | \Psi \rangle
= -\frac{e^2}{\hat{\rho}} \sum_{m'\nu'} \int d^3 \vec{r} \int d^3 \vec{r}' \phi_{m\nu}^*(\vec{r}') \phi_{m'\nu'}^*(\vec{r}) \frac{1}{|\vec{r} - \vec{r}'|}
\times \phi_{m\nu}(\vec{r}) \phi_{m'\nu'}(\vec{r}').$$
(23)

Only the exchange term remains in 1st order because the direct Coulomb term and the effective potential cancel out when the Hartree single-orbital wavefunctions have converged in the iteration associated with (15).

Total energy E to 1st order is given by,

$$E = \sum_{m\nu} \epsilon_{m\nu}^{(0)} + E^{(1)}, \tag{24}$$

$$E^{(1)} = \langle \Psi | H^{(1)} | \Psi \rangle$$

$$= -\frac{e^2}{2\hat{\rho}} \sum_{m\nu} \sum_{m'\nu'} \int d^3 \vec{r} \int d^3 \vec{r}'$$

$$\left(|\phi_{m\nu}(\vec{r})|^2 |\phi_{m'\nu'}(\vec{r}')|^2 \frac{1}{|\vec{r} - \vec{r}'|} + \phi_{m\nu}^*(\vec{r}') \phi_{m'\nu'}^*(\vec{r}) \frac{1}{|\vec{r} - \vec{r}'|} \phi_{m\nu}(\vec{r}) \phi_{m'\nu'}(\vec{r}') \right) (25)$$

In contrast, there remains part of the direct Coulomb term in $E^{(1)}$ following the way we have divided the Hamiltonian H into $H^{(0)}$ and $H^{(1)}$ in (3). However the applicability of type II perturbation is determined by the ratio $|\epsilon_{m\nu}^{(1)}/\epsilon_{m\nu}^{(0)}|$ as is discussed in §6.3.

5.5. Oscillator strengths

Oscillator strength in the length form for the transition $\Delta M = q$ is given as (M is the total magnetic quantum number $M = \sum_i m_j$,

$$f_{fi}^{(q)} = \frac{2m_e \hat{\rho}^2 E_{fi}}{\hbar^2} |\langle f| \sum_j r_j^{(q)} |i\rangle|^2,$$
 (26)

where

$$r_j^{(q)} = \sqrt{\frac{4\pi}{3}} r_j Y_{1q}(\theta_j, \phi_j).$$
 (27)

 Y_{lq} is the spherical harmonic. E_{fi} is the transition energy. Selection rule for the dipole-allowed transitions is:

$$\Delta m = \pm 1, \quad \Delta \nu = even$$

 $\Delta m = 0, \quad \Delta \nu = odd$

5.5.1. Dipole matrices

The dipole matrix elements $d^{(q)}$ in units of $\hat{\rho}$ are defined as,

$$d_{m\nu,m'\nu'}^{(q)} \equiv \langle m'\nu' | r^{(q)} | m\nu \rangle. \tag{28}$$

 $|m\nu\rangle$ and $|m'\nu'\rangle$ denote an orbital in initial and final state respectively. Using the orthonormality of Landau functions, dipole matrix elements are evaluated as,

$$d_{m\nu,m'\nu'}^{(0)} = \sum_{n,n'} c_{nm\nu} c_{n'm'\nu'} \delta_{m'm} \delta_{n'n}$$

$$\times \int dz \ f_{m'\nu'}^*(z) z \ f_{m\nu}(z), \qquad (29)$$

$$d_{m\nu,m'\nu'}^{(+1)} = -\sum_{n,n'} c_{nm\nu} c_{n'm'\nu'} \delta_{m'm+1} [\delta_{n'n+1} \sqrt{n+1} + \delta_{n'n} \sqrt{n+m}] \int dz \ f_{m'\nu'}^*(z) f_{m\nu}(z), \qquad (30)$$

$$d_{m\nu,m'\nu'}^{(-1)} = -\sum_{n,n'} c_{nm\nu} c_{n'm'\nu'} \delta_{m'm-1} [\delta_{n'n-1} \sqrt{n} + \delta_{n'n} \sqrt{n+m+1}] \int dz \ f_{m'\nu'}^*(z) f_{m\nu}(z). \qquad (31)$$

The longitudinal wavefunction for the initial and the final states are not quite orthogonal to each other due to differing electron configurations. Nevertheless we evaluated oscillator strengths for the single electron transitions using only the dipole matrix element of the transitioning electron. The error caused by this truncation is insignificant for one electron transitions.

6. VALIDITY AND OTHER PHYSICAL EFFECTS

6.1. Valid region in B-Z phase space

An expansion of the single-particle Hamiltonian in terms of cylindrical wavefunctions provides accurate results when $B > B_c$. As mentioned in §3 this is a statement that magnetic field effects dominate over Coulomb field effects. On the other hand, the perturbative treatment of higher Landau levels is valid when $|\tilde{h}^{(1)}| < |\tilde{h}^{(0)}|$. Since the nuclear term in equation (20) dominates the effective potential term, the condition $B > B_c$ is also sufficient to ensure the validity of a perturbative treatment of the higher Landau levels. Therefore, B_c sets a lower limit on the magnetic field for which our method is valid for tightly-bound electrons (i.e. in state (m,0)). In figure 2, we plot B_c for m=0-3 assuming $Z_{eff} \simeq Z-m$ for illustrative purposes. Loosely-bound electrons are well within the Landau regime due to their larger average distance to the nucleus. Therefore even at intermediate field strengths a cylindrical expansion combined with perturbative treatment of the higher Landau levels still provides accurate results for most electrons. The sharp decrease in B_c with increasing m, seen in figure 2, means that only those tightly-bound inner electrons with m = 0 - 3 will have significant configuration mixing. At higher quantum state m, the Landau regime, with its negligible configuration mixing, is quickly recovered.

6.2. Spin-flip transitions

As the magnetic field gets smaller, spin-flip transitions can take place, obviating the validity of the FSP approximation. The critical magnetic field strengths where spin-flip transitions take place (B_{sf}) were recently studied for atoms up to Z=10 by Ivanov & Schmelcher (2000). In a fairly wide range of magnetic field they computed the ground state energies of atoms in which the FSP approximation was removed – the electron spins were unrestricted. Using this study we found that B_{sf} could be fit by a polynomial function of Z. At $B < B_{sf}$ the assumption of antisymmetrized total spatial wave function breaks down. This sets another restriction on the validity of our method in the phase space of (B,Z) (figure 2).

6.3. Exchange term

Although the significance of the exchange term in the binding energy increases in the FSP approximation (Schmelcher et al. 1999), the exchange term can be treated perturbatively as long as it is smaller than the 0th order energy eigenvalues, i.e. $|\epsilon_{m\nu}^{(1)}| < |\epsilon_{m\nu}^{(0)}|$. We observed this inequality was satisfied for any single orbital in all the configurations computed. In the perturbation for the exchange term we did not perform calculations higher than 0th and 1st order for the wavefunctions and energy values because of the increasing complexity of the calculations. Also the naive inclusion of a 1st order perturbation into the wavefunctions breaks the wavefunctions orthogonality, requiring a further orthogonalization process for the single-orbital wavefunctions. The exact value of the wavefunction is not our primary concern, but rather the accuracy of the real physical observables such as energy values and oscillator strengths. For instance, errors on the energy levels caused by truncating the wavefunctions are actually small (§8.1). We use an explicit procedure to quantitatively correct the oscillator strengths in order to account for the deviation introduced by using Hartree rather than Hartree-Fock wavefunctions (§8.2).

6.4. Electron correlation

In reality the individual wavefunctions are not symmetric but distorted by the Coulomb coupling with other electrons. The Hartree and Hartree-Fock methods do not include electron correlation in the Schrödinger equation for each orbital. However, as the magnetic field increases, the electron correlation becomes less relevant (Schmelcher et al. 1999). The estimated error in our energies and oscillator strengths due to electron correlation is significantly smaller than 1% in the Landau regime.

6.5. Relativistic effects

The significance of relativistic effects is proportional to $\hbar \omega_B/m_e c^2$ or $E_B/m_e c^2$ where E_B is a binding energy. The former condition translates to B/B_{rel} ($B_{rel}=4.414\times10^{13}$ G), representing the degree of relativistic effects in the transverse motion of electrons. However, the shape of the Landau wavefuntion in the relativistic theory is the same as in the non-relativistic theory (Lai 2000). On the other hand, the electron becomes relativistic along the magnetic field when $E_B\sim m_e c^2$. However, the relativistic effects on the Coulomb binding energies remain negligible even at magnetic field strengths of up to 4.7×10^{13} G as determined by numerically solving Dirac's equation

for hydrogen (Lindgren & Virtamo 1979; Chen & Goldman 1992). Also, the second condition is relevant only to the inner orbitals which are not important for X-ray spectroscopy since their binding energies are high ($>10~\rm keV$).

6.6. Finite nuclear mass effects

In the presence of a magnetic field, the collective motion of an atom and its internal degrees of freedom are coupled, and this coupling modifies the electronics structure of the atom (Pavlov & Meszaros 1993; Potekhin 1994). Consequences of this coupling include distortion of the wavefunctions, violation of some dipole selection rules and line broadening. Most work on these finite nuclear mass effects has been performed on hydrogen atoms (Lai et al. 1992; Pavlov & Meszaros 1993; Potekhin 1994; Kopidakis et al. 1996; Potekhin 1998) and hydrogenic ions (Bezchastnov et al. 1998).

The immediate impact on our work is that the energy levels and oscillator strengths are affected by these collective effects. In this section we briefly review the collective motion and the theoretical framework for addressing it. In this paper we do not relax the assumption of an infinite nuclear mass in the Hamiltonian. This facilitates direct numeric comparison of our MCPH³ approach with other approaches for solving the strong magnetic field Hamiltonian, since they also assumed infinite nuclear mass. We do explain, in light of previous work on hydrogenic systems, how we will incorporate the collective motion into the MCPH³ technique in a subsequent paper. In the case of the bound-bound transitions of interest to us we describe the straightforward incorporation of finite nuclear mass into the oscillator strength calculation. This is appropriate since previous hydrogen work also included the effects of the finite nuclear mass on the oscillator strengths.

The finite nuclear mass treatment is quite complicated in hydrogen and has not really be dealt with previously for higher Z atoms. We outline in this section how substantial simplifications of this problem arise when considering both the specifics of higher Z systems in general and the requirements of X-ray spectroscopic modeling in particular.

6.6.1. Review of previous approaches to finite nuclear mass effects

When the nuclear mass is not assumed to be infinite the Hamiltonian, including a term for nuclear motion, can be separated into center-of-mass (CM) and relative coordinates by a canonical transformation, yielding

$$H \to H' = H_{cm} + H_{int} + H_c, \tag{32}$$

where H_{cm} and H_{int} are the Hamiltonian for the CM motion and the internal part. There is a scaling law for H_{int} from the infinite nuclear mass case (corresponding to the Hamiltonian in equation (2)) to the finite mass case (Pavlov-Verevkin & Zhilinskii 1980; Becken et al. 1999). Even when there is no translation motion of the atom, there is an additional term $m\hbar\Omega_B$ (m is the z-component of angular momentum and Ω_B is the cyclotron frequency of the nucleus) arising from the cyclotron motion of the nucleus (hereafter we call this term as the nuclear cyclotron term). Due to the nuclear cyclotron term, the large m

states are autoionized (Kopidakis et al. 1996). Since this term commutes with the Hamiltonian, it is easy to implement as an additive term in H_{int} . Less straightforward to handle is the coupling term H_c . This term arises because the motion of the CM through the magnetic field induces an electric field – the so-called motional Stark effect. The motional Stark field acts as a dipole electric field which increases the separation between electron and nucleus and therefore decreases the binding energy compared to the infinite nuclear mass case. H_c can be expressed as:

$$H_c = \frac{e}{Mc} (\vec{K} \times \vec{B}) \cdot \vec{r}, \tag{33}$$

where M is the nuclear mass and \vec{r} is the relative coordinate between the nucleus and the electron. $\vec{K} = \vec{\pi} - e(\vec{B} \times \vec{r})/c$ is the pseudomomentum, where $\vec{\pi} = \vec{p} + e\vec{A}/c$ represents the kinetic momentum. The pseudomomentum commutes with the Hamiltonian and therefore is a constant of motion. The pseudomomentum defines a separation between the guiding centers of the nucleus and the electron; $\vec{r}_c = \frac{c}{eB^2}(\vec{K} \times \vec{B})$. The components of the pseudomomentum commute for neutral atoms, while they do not commute for a charged system (Baye & Vincke 1990).

The motional Stark field breaks the cylindrical symmetry which is present by the central Coulomb field in the infinite nuclear mass case. As a result the system observables generally depend on K_{\perp} , the transverse component of the pseudomomentum. For instance, we express the binding energy of an electron in an orbital (m, ν) as $\epsilon_{m\nu}(K_{\perp})$. States can be classified according to the relative size of K_{\perp} compared to a critical pseudomomentum $K_c \sim (2M\epsilon_{m\nu}(0))^{1/2}$ and $\epsilon_{m\nu}(0)$ is the binding energy of the electron in a non-moving atom. When $K_{\perp} < K_c$ the central Coulomb field exceeds the Stark field; this is called a centered state. When $K_{\perp} > K_c$ the Stark field dominates and it separates the electron from its equilibrium (Coulomb) position around the nucleus; this is a decentered state.

Treatment of collective effects in the Hamiltonian depends on whether a state is centered or decentered. For decentered states a coordinate system $\vec{r}' = \vec{r} - \vec{r}_c$ is useful because the coupling term H_c becomes zero in the transformed Hamiltonian H'. Instead the nuclear Coulomb term is shifted by \vec{r}_c , requiring evaluation of matrix elements at each K_{\perp} . For nearly centered states the motional Stark effect can be treated by considering the coupling term H_c as a perturbation to the infinite nuclear mass solution (Pavlov & Meszaros 1993). In the perturbation method binding energy is given by,

$$\epsilon_{m\nu}(K_{\perp}) = \epsilon_{m\nu}(0) + \frac{K_{\perp}^2}{2M_{\mu\nu}^{\perp}}.$$
 (34)

 $M_{m\nu}^{\perp}$ is the transverse mass, which can be obtained by the 2nd order perturbation, since the bound states are non-degenerate. The transverse mass is larger than the atomic mass M (mass anisotropy).

Non-perturbative calculation was first studied by Vincke et al. (1992). Potekhin (1994) studied binding energies, oscillator strengths and size of moving hydrogen atom by the multi-configurational method. Potekhin (1998) obtained fitting formula based on the results of Potekhin (1994). Bezchastnov et al. (1998) investigated hydrogen-like helium by multi-configurational method with two particle

basis sets. For a charged system the collective motion is quantized by the cyclotron motion due to the non-zero net charge. Therefore atomic structure is characterized by the Landau numbers of the collective cyclotron motion instead of K_{\perp} . Baye & Vincke (1990) and Schmelcher (1995) have investigated a unified picture of general neutral and charged systems.

6.6.2. Effect of finite nuclear mass on X-ray spectral features in MCPH³

We have only considered the infinite nuclear mass case in this paper to validate MCPH³ against other methods, which did not consider collective effects in non-hydrogenic systems. However, we included a correction due to the nuclear cyclotron term for oscillator strengths of $\Delta m \neq 0$ transitions for hydrogen (mentioned elsewhere in §8.2). We outline here the program we will implement in a subsequent paper to accommodate these collective effects within the MCPH³ formalism.

First of all, the degree of motional Stark effect decreases monotonically with the nuclear mass M. In addition, the binding energy of the inner electrons increases as the nuclear charge Z becomes larger. Therefore, the tightlybound states are centered or nearly centered states. This allows us to adopt the perturbation method for centered states as employed by Pavlov & Meszaros (1993) and Lai & Salpeter (1995). This approach is fully compatible with MCPH³ but will set a constraint on the density range of applicability for a given temperature. In particular this approach is effective at higher densities where highly excited (decentered) states are destroyed by quasi-static electric fields from adjacent atoms and by collisions with fast free electrons (pressure ionization), or are autoionized due to the nuclear cyclotron term. As shown by Potekhin et al. (1999) the relative population of centered and decentered states in neutral hydrogen depends on B, ρ and T in a complicated manner. The range of validity of the perturbation theory will be the region of parameter space where centered states dominate. The range of parameter space in which a perturbative approach is valid will be much larger in the case of higher Z atoms compared to hydrogen because of the heavier nuclear mass involved. We also note that, at sufficiently high B, differences in the nuclear cyclotron term for different m states can be larger than the distances between single-orbital energy levels. This results in level mixing and sets constraint on the applicability of MCPH³. Taking into account these points the parameter space (B, Z, ρ, T) of validity will be the subject of our next paper to construct realistic atmosphere models.

A number of effects have been considered in the literature that are much less important for X-ray spectroscopy in the XMM-Newton and Chandra energy bands. For instance, as the motional Stark field decreases the binding energy spectral features are subject to redward line broadening (magnetic broadening, Pavlov & Meszaros (1993)). In addition, the Stark field breaks the cylindrical symmetry opening up new transitions that are forbidden according to the dipole selection rules for non-moving atom. Pavlov & Meszaros (1993) classified spectral features associated with the motional Stark effect as arising from high or low energy components. High energy components in the soft X-ray band consist of transitions from states of large

binding energy; they are centered states. On the other hand, the low energy components of Pavlov & Meszaros (1993) result from decentered state transitions leading to radiation in the optical—UV band. Consequently we will be able to apply the perturbation methods to the magnetic broadening for spectral features in the soft X-ray band.

7. Numerics

7.1. Spatial grid points and computation time

The main part of the iterative calculation is solving the eigenvalue equation (15) for each orbital and the numerical evaluation of the relevant integrals. We perform a finite element method, using a set of grid points $\{\rho_i\}$ $(N_{\rho}$ elements, grid interval $\Delta \rho_i$) and $\{z_j\}$ $(N_z$ elements, grid interval Δz_i) for the transverse and longitudinal direction respectively. Since a (m, ν) state is localized around $(2m+1)^{1/2}\hat{\rho}$ with the width $\sim \hat{\rho}$ in the transverse direction (Meszaros 1992), the transverse size of $10\hat{\rho}$ is large enough for Z < 30. We precalculated all the relevant kernels (nuclear, direct and exchange) as a function of z by integrating over the grid points $\{\rho_i\}$, since the kernels are independent of B when we use the cyclotron radius for the unit of length. See the appendix for the evaluation of kernels. We used a set of uniform grid points for $\{\rho_i\}$ with $N_{\rho}=10^3$ and $\Delta\rho_i=10^{-2}$. We evaluated the integrals by a five-point Newton-Cotes integration formula. Numerical error associated with the kernel integrals is negligibly small. Prior to the calculation for a given electron configuration, the kernels are read from the database comprised of about 3×10^5 lines of floating-point numbers. The kernel database is extended over m = 0 - 30 for singleconfigurational calculation and n = 1 - 7 for the magnetic quantum numbers m = 0 - 5 for multi-configurational calculation. This is sufficiently large for Z = 1 - 26 in the Landau regime. The algorithm of our atomic calculation is presented in figure 3.

When solving an eigenvalue equation for each orbital by Numerov algorithm (Koonin 1986), we confined the longitudinal coordinate to $0 \le z \le L$, with a sufficiently large size of the integration box L, because $f_{m\nu}(z)$ is symmetric regardless of the electron correlation. Boundary conditions are : $f_{m\nu}(z=0)=0$ (Dirichlet condition) for odd ν 's, $f'_{m\nu}(z=0)=0$ for even ν 's (Neumann condition) and $f_{m\nu}(z=L)=0$ for all ν 's. In contrast to the transverse direction, the characteristic length of longitudinal wavefunctions varies greatly with ν (Ruderman 1971) (a_0 is the Bohr radius, $a_0/\hat{\rho}=\sqrt{2}\beta^{1/2}$).

$$L \sim (a_0/Z\hat{\rho}) \ln (a_0/Z\hat{\rho}) \qquad (\nu = 0)$$
$$\sim a_0 \nu^2/\hat{\rho} \qquad (\nu > 0)$$

In compensation for saving computation time from the kernel calculation, we confront the difficulty of the B-dependent size of the integration box as we keep the fine grid intervals. Inner tightly-bound orbitals require finer grid points (especially for high Z atoms), while wavefunctions of outer orbitals require large extension in integration box, with L as large as ~ 1000 depending on B, Z and ν . As the results are sensitive to the grid intervals, uniform grid points are not appropriate for an atom mixed with tightly-bound and loosely-bound electrons unless we have a large number of grid points N_{grid} (meaning large computation time). Therefore, we adopt the non-uniform grid

points : $z_j = g(\tilde{z}_j)$ of Ivanov (1994). $\{\tilde{z}_j\}$ is a set of uniform grid points on which the equation (15) is solved, while $\{z_i\}$ is a set of actual non-uniform grid points. A function $g(\tilde{z})$ must be chosen so that the grid intervals Δz_j become denser near the origin and sparser at large z. Upon the mapping of coordinates, the equation (15) must be transformed into an appropriate form in terms of a new set of grid points $\{\tilde{z}_i\}$. For some of the loosely-bound orbitals, we do not know ab initio where a wavefunction changes steeply, but they do not require finer grid points compared to tightly-bound states. Therefore, we used uniform grid points with the interval $\Delta z_j \sim 0.5-0.8$. It reduces the number of grid points significantly to $N_z = 70-200$ for tightly-bound orbitals and $N_z = 70 - 1000$ for looselybound orbitals. Note that most electrons are usually in tightly-bound orbitals while a few loosely-bound orbitals are occupied by excited states and the ground states of high Z atoms. Keeping the same set of grid points for different electron configurations for different B and Z is still a difficult task. We adjust the grid points, if necessary, after the 1st iteration.

Computation time is proportional to $N_{grid}^2 \times N_e^2 \times N_{iter}$ for the self-consistent methods due to the coupling between electrons (N_e is the number of electrons, N_{iter} is the number of iterations). Use of a one-dimensional Hartree equation is far superior to 2DHF ($N_{grid} = N_{\rho} \times N_z = 65 \times 65 = 4225$) (Ivanov & Schmelcher 2000) in terms of the computation time. Miller & Neuhauser (1991) adopted uniform grid points ($N_z = 500 - 1000$ and $\Delta z = 0.2 - 0.8$) for most of their electron configurations computed, suffering the numerical inaccuracy caused by the coarse grid points, as pointed out by Thurner et al. (1993).

7.2. Convergence and numerical errors

Our initial guess for the longitudinal wavefunction of the (m, ν) orbital is adopted from restricted variational studies (Flowers et al. 1977).

$$f_{m\nu}(z) \propto z^{\nu} e^{-a_{m\nu}|z|} \tag{35}$$

The final results do not change with our initial choice of $\{a_{m\nu}\}$ varying from 0.1 to 10. Energy values converge to less than 1% after the 2nd iteration and less than 0.1% after the 4th iteration, although convergence speed becomes slow as N_e increases (figure 4). Therefore, estimations of convergence speed from hydrogen results (Miller & Neuhauser 1991) are not correct. Convergence speed for a 2DHF calculation will be slower than in the one-dimensional Hartree method.

Upon the evaluation of the direct and exchange terms, we found that the coupling terms between different n>0 states are negligible (< 0.1%). Therefore, we did not include the contribution from n>0 Landau states of other orbitals (setting $\tilde{n}=\tilde{n}'=0$ in (A9) and (A10) in the appendix), reducing the computation time when evaluating the 1st order total energy. The numerical error is overall less than 0.1%.

8. RESULTS

8.1. Energy values and ground state configurations

We have computed total energies for ground states and several excited states at representative magnetic fields. The computed energies match with the previously most accurate values (e.g. 2DHF) with less than 1% deviation. In general, model-dependent total energy is closer to the exact value when it is lower than other models. However, the computed energy values can be lower than the exact values due to numerical error or inconsistency in atomic models. At β_Z close to 1, our energy values are actually lower than the previous results known to be accurate to 4 digits. This is because higher Landau states of the innermost electrons are no longer perturbations on the n=0 state. Therefore, perturbative method may provide total energies lower than the previous accurate data. Nevertheless, we listed the multi-configurational results as long as the discrepancy is less than 1%.

8.1.1. Hydrogen

We present the energies for ground states and several excited states in comparison with the multi-configurational Hartree-Fock method (MCHF hereafter) (Ruder et al. 1994) (table 1, 2). They fully included higher Landau levels up to n=12 in the Hartree-Fock equation. We produced fairly good energy values with <1% deviation from MCHF.

8.1.2. *Helium*

We compare our results with 1DHF (Thurner et al. 1993; Miller & Neuhauser 1991) and UHF (Jones et al. 1999b) for the ground state and several excited states (table 3, 4). The ground state configuration for helium is $(m,\nu)=(0,0),(1,0)$ in the Landau regime. Our single-configurational total energies (excluding n>0 Landau levels) match well with 1DHF results (Thurner et al. 1993) by <0.5%. Our multi-configurational total energies are lower than 1DHF by $\sim 1-5\%$ at $\beta_Z < 10$ and higher than UHF by <1% at $\beta_Z > 1$.

8.1.3. High Z atoms

For Z > 2 atoms, published atomic data is scarce (Neuhauser et al. 1987; Ivanov & Schmelcher 2000). First of all, we searched for the ground state configurations of neutral atoms Z = 2 - 26 at some representative field strengths [table 5.6]. In the limit of $B \to \infty$, the ground state configuration is such that all the bound electrons are in tightly-bound orbitals $(m, \nu) = (0, 0), (1, 0)...(N_e - 1, 0)$. With decreasing B, the spatial crossover takes place, i.e. having electrons in loosely-bound orbitals rather than in outer tightly-bound orbitals, lowers the total energy. A $\nu = 2$ orbital may form the ground state configuration because a $\nu = 2$ orbital can be closer to the nucleus than $\nu = 1$ orbitals due to the electron screening (Jones 1985b). However, we did not find any ground state configurations with $\nu = 2$ orbitals at the magnetic fields in tables 5 and 6. Several spatial crossovers take place before the spin-flip transition sets in, as we observed for high Z atoms (Ivanov & Schmelcher 2000). Ivanov & Schmelcher (2000) investigated the ground state configurations at $\beta \sim 10^{-1} - 10^4$ for Z = 1 - 10 atoms. For Z > 10 atoms, only Neuhauser et al. (1987) provided the ground state configurations and the total energies among the self-consistent methods.

Our single-configurational total energies match very well with 1DHF (Neuhauser et al. 1987) up to Z=5, while 1DHF total energies become higher than our values by

at most 1% at Z > 5. This is probably because their grid points are not sufficiently fine for inner electrons in high Z atoms. Our multi-configurational results are 5-10% lower than 1DHF at $\beta_Z \leq 10$ and a few % lower at $\beta_Z \leq 100$. Some of their ground state energies are even higher than our multi-configurational energy of several excited states.

Jones (1986) studied the ground state energy for several high Z neutral atoms by DF. Their results are a few % lower than our results and 2DHF for the ground states of several atoms, while they fixed n=0 (table 6). Ground state energies obtained by DF are highly dependent on the form of the exchange-correlation density functionals (Jones 1985a), even though DF can relatively easily implement the exchange and electron correlation terms in the local density approximation.

Up to Z = 10, our multi-configurational ground state energies are higher than 2DHF results by < 1% overall at $\beta_Z > 1$. Even though 2DHF claims no numerical errors by the use of the Richardson extrapolation method, this difference could be attributed to the fact that we did not include the 2nd order perturbation in the total energy. The errors are expected to come mainly from the inner electrons but to be smaller for outer electrons. However, the inner electrons of high Z atoms are irrelevant to X-ray spectroscopy since their binding energy is relatively high (> 10 keV), while the inner electrons in low Z atoms can contribute to the opacities in the X-ray band. The accuracy in total energies within 1% in comparison with 2DHF results is sufficient for the identification of the potential atomic lines or edges. Our energies as well as the 0th order wavefunctions can be improved by adding an appropriate local exchange term to a single-orbital Hartree equation. In contrast, empirical density functionals for the exchange term in the Landau regime are not known presently.

8.2. Oscillator strengths

Compared to energy values, oscillator strengths are subject to more atomic model dependent uncertainties. This is because atomic models are usually optimized for minimizing the total energy. The completeness of the orbital wavefunctions represented by Thomus-Kuhn rules is a secondary issue. Errors in transition energy values can affect the oscillator strengths. For the candidate strong transitions, 10% accuracy in the oscillator strengths is sufficient, considering that spectral features can undergo a number of broadening effects (Rajagopal et al. 1997). For the same reasons, we do not consider transitions other than dipoleallowed. For hydrogen, we compare to the results from MCHF (Ruder et al. 1994) and we included a correction by the proton cyclotron term for $\Delta m \neq 0$ transitions. Consequently, the oscillator strengths match fairly well with their results (table 7).

Data for oscillator strengths at Z>1 were found only for 1DHF. Miller (1990) published data at Z=2,6 for bound-bound transitions, while Ruder et al. (1994) obtained the oscillator strengths only for helium-like atoms. It turns out that tight-tight transitions match with 1DHF very well, while the oscillator strengths for tight-loose transitions are consistently larger than 1DHF results by 10-50 %. The most likely explanation is that we did

not include the exchange effects in the orbital wavefunction. In the antisymmetrized Hartree total wavefunctions, electrons are closer to each other than in the Hartree-Fock total wavefunctions. As exchange effects are larger for a pair of closer electrons, tightly-bound electrons are more deviant from Hartree-Fock orbitals. This discrepancy is small for the inner tightly-bound electrons since their behavior is mainly determined by the Coulomb attraction from the nucleus. Also, it is very small for a loosely-bound electron simply because it is far from other electrons, unless there are other loosely-bound electrons nearby. For tight-tight transitions, a transitioning electron (usually the outermost tightly-bound electron) in the Hartree scheme is closer to the nucleus than in the Hartree-Fock scheme both in the initial and final state. This deviation cancels out when we evaluate the oscillator strengths by the length form because a change in the spatial distribution of the electron associated with the atomic transition is about the same in the Hartree and the Hartree-Fock picture. However, for tight-loose transitions, the deviation in the initial state remains in the oscillator strengths and it gives us the consistently larger oscillator strengths because the Hartree scheme requires larger change in the spatial distribution compared to the Hartree-Fock scheme.

A well-defined measure of this deviation associated with each bound electron is the ratio of the exchange term to the Hartree single-orbital energy, i.e. $r_{ex} = |\epsilon_{m\nu}^{(1)}/\epsilon_{m\nu}^{(0)}|$. Therefore, we introduced a correction to the oscillator strengths for the tight-loose transitions by the amount of r_{ex} . The same correction is applicable when size of atoms or ions is required to include non-ideal effects, for instance through the excluded-volume term (Potekhin et al. 1999). In contrast to hydrogen case, we did not include the finite nuclear mass correction since the previous results for comparison assumed the infinite nuclear mass. As a result, the corrected oscillator strengths match with 1DHF results within 10% for different tight-loose transitions of helium and carbon at various magnetic fields (table 8, 9). The discrepancy at small β_Z is due to the finite occupation in higher Landau levels, which is not included in 1DHF but is included in MCPH³. Although comparisons are available only for helium and carbon due to few publications on oscillator strengths for Z > 1, the numerical results in tables 8 and 9 based on this physically reasonable correction, strongly support that oscillator strengths are calculated with 10% accuracy for other atoms up to

9. FUTURE WORK

Construction of an extensive atomic data base from the method presented in this article is in progress. It consists of energies and oscillator strengths for a large number of grid points in B. Based on the atomic data, equation of state and opacity tables will be constructed in the phase space of (B, ρ, T, Z) covering the typical parameter values for cooling neutron stars.

We are grateful to Ehud Behar for careful reading the manuscript. This work was partially supported by NASA grant NAG5-7737.

APPENDIX

EVALUATION OF POTENTIALS AND ENERGIES

Analytical expression of potentials and energies

In order to avoid the complications caused by the r^{-1} cusp at the origin, we expanded the terms r^{-1} and $|\vec{r}-\vec{r}'|^{-1}$ appearing in the potentials by the Bessel functions $J_m(x)$ (Flowers et al. 1977). $L_m(x)$, $L_m^n(x)$ denote the Laguerre function and associated Laguerre function respectively. Hereafter, $\int dk = \int_0^\infty dk$, $\int dz = \int_{-\infty}^\infty dz$, $\int d\rho = \int_0^\infty d\rho$, $\int d\phi = \int_0^{2\pi} d\phi$.

$$r^{-1} = \frac{1}{\sqrt{\rho^2 + z^2}} = \int dk J_0(k\rho) e^{-k|z|},$$

$$|\vec{r} - \vec{r}'|^{-1} = \frac{1}{\sqrt{\rho^2 + {\rho'}^2 - 2\rho\rho'\cos(\phi - \phi') + (z - z')^2}}$$

$$= \sum_{k=0}^{\infty} \int dk \ e^{im(\phi - \phi')} J_m(k\rho) J_m(k\rho') e^{-k|z - z'|}.$$
(A1)

For the single-configurational potentials,

$$V_{nuc}(z) = -\frac{Ze^2}{\hat{\rho}} V_{m00}(z),$$
 (A3)

$$V_{eff}(z) = \frac{e^2}{\hat{\rho}} \sum_{m'\nu'} \int dz' \, D_{m'00}^{m00}(z - z') |f_{m'\nu'}(z')|^2, \tag{A4}$$

where nuclear and direct kernels are defined as

$$V_{mnn'}(z) \equiv \int \rho d\rho \int d\phi \, \Phi_{n'm}^*(\rho,\phi) \Phi_{nm}(\rho,\phi) \, \frac{1}{r}, \tag{A5}$$

$$D_{m'\tilde{n}\tilde{n}'}^{mnn'}(z-z') \equiv \int \rho d\rho \int d\phi \int \rho' d\rho' \int d\phi' \, \Phi_{\tilde{n}m'}^*(\rho',\phi') \Phi_{\tilde{n}'m'}(\rho',\phi')$$

$$\times \Phi_{nm}(\rho,\phi) \Phi_{n'm}^*(\rho,\phi) \frac{1}{|\vec{r}-\vec{r}'|}. \tag{A6}$$

The matrix elements for the multi-configurational calculation are:

$$\langle nm\nu|V_{nuc}(\vec{r})|n'm\nu\rangle = -\frac{Ze^2}{\hat{\rho}} \int dz \ V_{mnn'}(z)|f_{m\nu}(z)|^2, \tag{A7}$$

$$\langle nm\nu|V_{eff}(\vec{r})|n'm\nu\rangle = \frac{e^2}{\hat{\rho}} \sum_{m'\nu'} \sum_{\tilde{n},\tilde{n}'} c_{\tilde{n}m'\nu'}c_{\tilde{n}'m'\nu'} \int dz \ D_{m'\tilde{n}\tilde{n}'}^{mnn'}(z-z')$$

$$\times |f_{m\nu}(z)|^2 |f_{m'\nu'}(z')|^2. \tag{A8}$$

1st order perturbation of single-orbital energy and total energy are given as,

$$\epsilon_{m\nu}^{(1)} = -\frac{e^2}{\hat{\rho}} \sum_{m'\nu'} \sum_{n,n'} \sum_{\tilde{n},\tilde{n}'} c_{nm\nu} c_{n'm\nu} c_{\tilde{n}m'\nu'} c_{\tilde{n}'m'\nu'} \int dz \int dz' E_{m'\tilde{n}\tilde{n}'}^{mnn'}(z-z')
\times f_{m\nu}(z) f_{m'\nu'}(z') f_{m'\nu'}^*(z) f_{m\nu}^*(z'),$$
(A9)
$$E^{(1)} = -\frac{e^2}{2\hat{\rho}} \sum_{m\nu} \sum_{m'\nu'} \sum_{n,n'} \sum_{\tilde{n},\tilde{n}'} c_{nm\nu} c_{n'm\nu} c_{\tilde{n}m'\nu'} c_{\tilde{n}'m'\nu'} \int dz \int dz'
\left(D_{m'\tilde{n}\tilde{n}'}^{mnn'}(z-z') |f_{m\nu}(z)|^2 |f_{m'\nu'}(z')|^2
+ E_{m'\tilde{n}\tilde{n}'}^{mnn'}(z-z') f_{m\nu}(z) f_{m'\nu'}(z') f_{m'\nu'}^*(z) f_{m\nu}^*(z') \right),$$
(A10)

where exchange kernels are defined as

$$E_{m'\tilde{n}\tilde{n}'}^{mnn'}(z-z') \equiv \int \rho d\rho \int d\phi \int \rho' d\rho' \int d\phi' \, \Phi_{n'm}^*(\rho',\phi') \Phi_{\tilde{n}'m'}^*(\rho',\phi')$$

$$\times \frac{1}{|\vec{r}-\vec{r}'|} \Phi_{nm}(\rho,\phi) \Phi_{\tilde{n}m'}(\rho,\phi). \tag{A11}$$

Nuclear and direct kernels

$$V_{mnn'}(z) = \int dk \ e^{-k|z|} \zeta_{nn'}^m(k), \tag{A12}$$

$$D_{\tilde{m}\tilde{n}\tilde{n}'}^{mnn'}(z-z') = \int dk \ e^{-k|z-z'|} \zeta_{nn'}^{m}(k) \zeta_{\tilde{n}\tilde{n}'}^{\tilde{m}}(k). \tag{A13}$$

The zeta function is defined as,

$$\zeta_{nn'}^{m}(k) \equiv \int \rho d\rho \int d\phi \, \Phi_{nm}^{*}(\rho,\phi) \Phi_{n'm}(\rho,\phi) J_{0}(k\rho),
= \left[\frac{n!n'!}{2^{2m}(n+m)!(n'+m')!} \right]^{1/2} \int d\rho \, \rho^{2m+1} e^{-\rho^{2}/2}
\times L_{n}^{m} \left(\frac{\rho^{2}}{2} \right) L_{n'}^{m} \left(\frac{\rho^{2}}{2} \right) J_{0}(k\rho).$$
(A14)

 ζ functions are analytically computed for some special cases.

$$\zeta_{00}^m(k) = L_m\left(\frac{k^2}{2}\right)e^{-k^2/2},$$
(A15)

$$\zeta_{nn'}^{0}(k) = (-1)^{n+n'} e^{-k^2/2} L_n^{n'-n} \left(\frac{k^2}{2}\right) L_{n'}^{n-n'} \left(\frac{k^2}{2}\right). \tag{A16}$$

The rest of the ζ functions are computed by the following recursion relation.

$$\zeta_{nn'}^{m}(k) = \sum_{n''=0}^{n'} \left[\frac{n'!(n''+m-1)!}{n''!(n'+m)!} \right]^{1/2} \left[\sqrt{n+m} \, \zeta_{nn''}^{m-1}(k) - \sqrt{n+1} \, \zeta_{n+1n''}^{m-1}(k) \right], \tag{A17}$$

$$\zeta_{n'n}^m(k) = \zeta_{nn'}^m(k). \tag{A18}$$

Exchange kernels

$$E_{m'\tilde{n}\tilde{n}'}^{mnn'}(z-z') = \int dk \ e^{-k|z-z'|} \eta_{mn}^{m'\tilde{n}}(k) \eta_{mn'}^{m'\tilde{n}'}(k). \tag{A19}$$

The eta function is defined as,

$$\eta_{mn}^{m'n'}(k) \equiv \int \rho d\rho \int d\phi \, \Phi_{nm}^*(\rho,\phi) \Phi_{n'm'}(\rho,\phi) J_{m'-m}(k\rho)
= \left[\frac{n!n'!}{2^{m+m'}(n+m)!(n'+m')!} \right]^{1/2} \int d\rho \, \rho^{m+m'+1} e^{-\rho^2/2}
\times L_n^m \left(\frac{\rho^2}{2} \right) L_{n'}^{m'} \left(\frac{\rho^2}{2} \right) J_{m'-m}(k\rho).$$
(A20)

 η functions are analytically computed for some special cases.

$$\eta_{mn}^{0n'}(k) = (-1)^{n+n'} \left[\frac{n!}{2^m (n+m)!} \right]^{1/2} k^m e^{-k^2/2} L_n^{n'-n} \left(\frac{k^2}{2} \right) L_{n'}^{m+n-n'} \left(\frac{k^2}{2} \right). \tag{A21}$$

The rest of the η functions are computed by the following recursion relation.

$$\eta_{mn}^{m'n'}(k) = \sum_{n''=0}^{n'} \left[\frac{n'!(n''+m-1)!}{n''!(n'+m)!} \right]^{1/2} \left[\sqrt{2(m'-m-1)^2} \frac{\eta_{mn}^{m'-1n''}(k)}{k} - \sqrt{n+m+1} \eta_{m+1n}^{m'-1n''}(k) + \sqrt{2n} \eta_{m+1n-1}^{m'-1n''}(k) \right],$$
(A22)

$$\eta_{m'n}^{mn'}(k) = \eta_{mn'}^{m'n}(k) = \left[\frac{(n+m')!(n'+m)!}{(n+m)!(n'+m')!}\right]^{1/2} \eta_{mn}^{m'n'}(k). \tag{A23}$$

REFERENCES

Abrahams, A. M. & Shapiro, S. L. 1991, ApJ, 382, 233 Alcock, C. & Illarionov, A. 1980, ApJ, 235, 534 Baye, D. & Vincke, M. 1990, Phys. Rev. A, 42, 391 Becken, W. & Schmelcher, P. 2000, J. Phys. B, 33, 545

—. 2001, Phys. Rev. A, 63, 0a4+ Becken, W., Schmelcher, P., & Diakonos, F. K. 1999, J. Phys. B, 32, 1557

Becker, W. & Trümper, J. 1997, A&A, 326, 682

Bezchastnov, V. G., Pavlov, G. G., & Ventura, J. 1998, Phys. Rev. A, 58, 180

Camilo, F., Thorsett, S. E., & Kulkarni, S. R. 1994, ApJ, 421, L15 Chen, H., Ruderman, M. A., & Sutherland, P. G. 1974, ApJ, 191, 473

Chen, Z. & Goldman, S. P. 1992, Phys. Rev. A, 45, 1722 Chevalier, R. A. 1996, ApJ, 459, 322

Demeur, M., Heenen, P., & Godefroid, M. 1994, Phys. Rev. A, 49, 176

Flowers, E. G., Ruderman, M. A., Lee, J. ., Sutherland, P. G., Hillebrandt, W., & Mueller, E. 1977, ApJ, 215, 291 Forster, H., Strupat, W., Rosner, W., Wunner, G., Ruder, H., & Herold, H. 1984, J. Phys. B, 17, 1301

Glasser, M. L. 1975, ApJ, 199, 206

Glasser, M. L. & Kaplan, J. I. 1975, ApJ, 199, 208

Hewish, A. S., Bell, A. J., Pilkington, J. D. H., Scott, P. F., & Collins, R. A. 1968, Nature, 217, 709

Ho, W. C. G. & Lai, D. 2001, preprint (astro-ph/0104199)

Holas, A. & March, N. H. 1997, Phys. Rev. A, 56, 4595 Hylleraas, E. A. 1930, Z. Physik, 65, 209 Ivanov, M. V. 1994, J. Phys. B, 27, 4513 Ivanov, M. V. & Schmelcher, P. 1998, Phys. Rev. A, 57, 3793

-. 1999, Phys. Rev. A, 60, 3558

2000, Phys. Rev. A, 61, 022505 Johnsen, K. & Yngvason, J. 1996, Phys. Rev. A, 54, 1936

Jones, M. D., Ortiz, G., & Ceperley, D. M. 1997, Phys. Rev. E, 55,

—. 1999a, A&A, 343, L91

. 1999b, Phys. Rev. A, 59, 2875

Jones, P. B. 1985a, Phys. Rev. Lett., 55, 1338

—. 1985b, MNRAS, 216, 503 —. 1986, MNRAS, 218, 477 Jordan, S., Schmelcher, P., Becken, W., & Schweizer, W. 1998, A&A, 336, L33 Koonin, S. E. 1986, Computational Physics (Benjamin/Cummings,

Menlo Park, California) Kopidakis, N., Ventura, J., & Herold, H. 1996, A&A, 308, 747 Kössl, D., Wolff, R. G., Müller, E., & Hillebrandt, W. 1988, A&A, 205, 347

Lai, D. 2000, preprint (astro-ph/0009333)
 Lai, D. & Salpeter, E. E. 1995, Phys. Rev. A, 52, 2611

-. 1996, Phys. Rev. A, 53, 152 -. 1997, ApJ, 491, 270

Lai, D., Salpeter, E. E., & Shapiro, S. L. 1992, Phys. Rev. A, 45,

Landau, L. D. & Lifshitz, E. M. 1965, Quantum mechanics (Course of theoretical physics, Oxford: Pergamon Press, 1965) Lieb, E. H., Solovej, J. P., & Yngvason, J. 1992, Phys. Rev. Lett.,

Lindgren, K. A. U. & Virtamo, J. T. 1979, J. Phys. B, 12, 3465 Meszaros, P. 1992, High-energy radiation from magnetized neutron stars (Theoretical Astrophysics, Chicago: University of Chicago

Press, —c1992) Miller, M. C. 1990, PhD thesis, California Inst. of Tech., Pasadena. —. 1992, MNRAS, 255, 129

Miller, M. C. & Neuhauser, D. 1991, MNRAS, 253, 107 Müller, E. 1984, A&A, 130, 415

Neuhauser, D., Koonin, S. E., & Langanke, K. 1987, Phys. Rev. A, 36, 4163

Neuhauser, D., Langanke, K., & Koonin, S. E. 1986, Phys. Rev. A, 33, 2084

Ortiz, G., Jones, M. D., & Ceperley, D. M. 1995, Phys. Rev. A, 52, 3405

Ostriker, J. P. & Gunn, J. E. 1969, Nature, 221, 454

Özel, F. 2001, preprint (astro-ph/0103227)

Paerels, F., Mori, K., Motch, C., Haberl, F., Zavlin, V. E., Zane, S., Ramsay, G., Cropper, M., & Brinkman, B. 2001, A&A, 365, L298 Page, D. 1998, in NATO ASIC Proc. 515: The Many Faces of

Neutron Stars., 539
Pavlov, G. G. & Meszaros, P. 1993, ApJ, 416, 752
Pavlov, G. G., Shibanov, Y. A., Zavlin, V. E., & Meyer, R. D. 1995, in The Lives of the Neutron Stars. Proceedings of the NATO Advanced Study Institute on the Lives of the Neutron Stars, Publisher, Kluwer Academic, Dordrecht, The Netherlands,

Stars, Publisher, Kluwer Academic, Dordrecht, The Netherlands, Boston, Massachusetts, 1995. p.71
Pavlov, G. G., Zavlin, V. E., Sanwal, D., Burwitz, V., & Garmire, G. 2001, ApJ, 552, L129
Pavlov-Verevkin, V. B. & Zhilinskii, B. 1980, Phys. Lett. A, 78, 244
Pons, J. A., Walter, F. W., Lattimer, J. M., & Prakash, M. 2000, AAS/High Energy Astrophysics Division, 32, 3314
Pottekkin, A. V. 1904. I. Phys. B, 27, 1072.

AAS/ Right Energy Astrophysics Division, 52, 5314

Potekhin, A. Y. 1994, J. Phys. B, 27, 1073

— . 1998, J. Phys. B, 31, 49

Potekhin, A. Y., Chabrier, G., & Shibanov, Y. A. 1999,
Phys. Rev. E, 60, 2193

Rajagopal, M. & Romani, R. W. 1996, ApJ, 461, 327

Rajagopal, M., Romani, R. W., & Miller, M. C. 1997, ApJ, 479, 347

Relovsky, B. M. & Ruder, H. 1996, Phys. Rev. A, 53, 4068

Rögnvaldsson, O. E., Fushiki, L. Gudmundsson, E. H., Pethick Rögnvaldsson, O. E., Fushiki, I., Gudmundsson, E. H., Pethick,

C. J., & Yngvason, J. 1993, ApJ, 416, 276 Romani, R. W. 1987, ApJ, 313, 718 Rösner, W., Wunner, G., Herold, H., & Ruder, H. 1984, J. Phys. B, 17, 29

Ruder, H., Wunner, G., Herold, H., & Geyer, F. 1994, Atoms in Strong Magnetic Fields. Quantum Mechanical Treatment and Applications in Astrophysics and Quantum Chaos (X, 309 pp. 93 figs.. Springer-Verlag Berlin Heidelberg New York.)

Ruderman, M. A. 1971, Phys. Rev. Lett., 27, 1306

Salpeter, E. E. 1998, Journal de Physique, 10, 11285 Schmelcher, P. 1995, Phys. Rev. A, 52, 130 Schmelcher, P., Ivanov, M. V., & Becken, W. 1999, Phys. Rev. A, 59, 3424

Scrinzi, A. 1998, Phys. Rev. A, 58, 3879 Skjervold, J. E. & Ostgaard, E. 1984, Phys. Scr, 29, 543 Steinberg, M., Ortner, J., & Ebeling, W. 1998, Phys. Rev. E, 58,

Thorolfsson, A., Rögnvaldsson, O. E., Yngvason, J., & Gudmundsson, E. H. 1998, ApJ, 502, 847

Thurner, G., Korbel, H., Braun, M., Herold, H., Ruder, H., &

Wunner, G. 1993, J. Phys. B, 26, 4719
Trümper, J., Pietsch, W., Reppin, C., Voges, W., Staubert, R., & Kendziorra, E. 1978, ApJ, 219, L105
Tsuruta, S. 1995, in The Lives of the Neutron Stars. Proceedings of

the NATO Advanced Study Institute on the Lives of the Neutron Stars, Publisher, Kluwer Academic, Dordrecht, The Netherlands,

Boston, Massachusetts, 1995. p.133 Vincke, M., LeDourneuf, M., & Baye, D. 1992, Journal of Physics B

Atomic Molecular Physics, 25, 2787

Wheaton, W. A., Doty, J. P., Primini, F. A., Cooke, B. A., Dobson, C. A., Goldman, A., Hecht, M., Howe, S. K., Hoffman, J. A., & Scheepmaker, A. 1979, Nature, 282, 240

Woosley, S. E. & Weaver, T. A. 1986, ARA&A, 24, 205

Yakovlev, D. G., Levenfish, K. P., & Shibanov, Y. A. 1999, Physics-Uspekhi, 42, 737

Zane, S., Turolla, R., & Treves, A. 2000, ApJ, 537, 387 Zavlin, V. E. & Pavlov, G. G. 1998, A&A, 329, 583 Zavlin, V. E., Pavlov, G. G., & Shibanov, Y. A. 1996, A&A, 315,

FIG. 1.— Comparison of various atomic models in the phase diagram of Z and β_Z . 1DHF = Hartree-Fock method with the adiabatic approximation (Neuhauser et al. 1986). 2DHF = Two-dimensional Hartree-Fock method (Ivanov & Schmelcher 2000). DF = Density functional method. TFD = Thomas-Fermi-Dirac method.

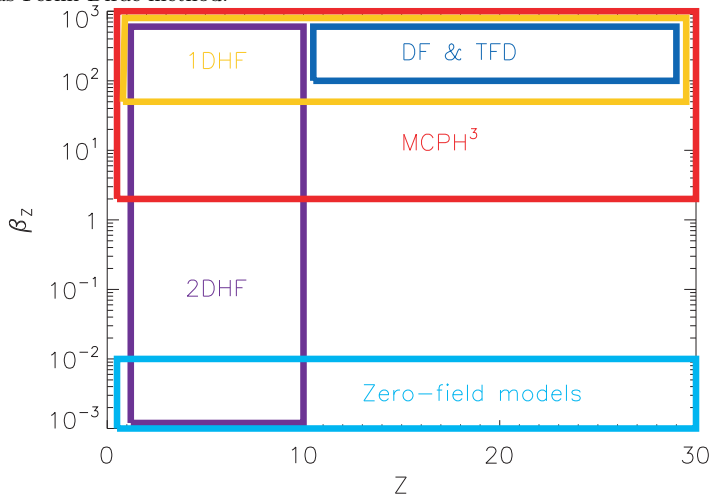
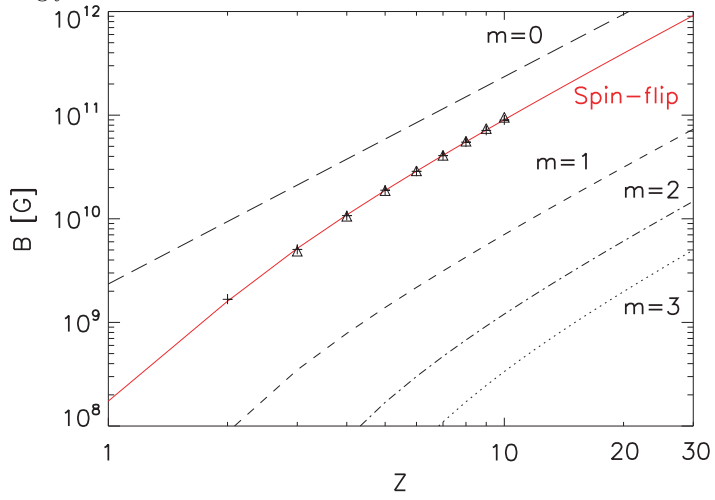


Fig. 2.— Critical magnetic field B_c for a tightly-bound orbital (m,0) and the spin-flip transition field strength B_{sf} . We assumed $Z_{eff} \simeq Z-m$ for illustrative purpose. We did a polynomial fit to the spin-flip field strengths obtained by Ivanov & Schmelcher (2000). $B_{sf}=1.7\times 10^9$ G for Z=2, $B_{sf}=9.6\times 10^{10}$ G for Z=10 and $B_{sf}=6.8\times 10^{11}$ G for Z=26. Triangle points represent B_{sf} for neutral atoms, while crossed points are for singly-ionized atoms.



 $\label{table 1} {\bf Table \ 1}$ Energies of tightly-bound states for hydrogen.

(m, ν)	(0,0)		(1,0)		(2,0)		(3,0)	
β	Present work	$Ruder^a$	Present work	Ruder	Present work	Ruder	Present work	Ruder
1	28.10	$27.82^{\rm b}$	16.33	$16.32^{\rm b}$	12.81	$12.82^{\rm b}$	10.84	$10.97^{\rm b}$
2	34.53	$34.85^{\rm b}$	21.38	$21.44^{ m b}$	16.84	$17.06^{\rm b}$	14.57	14.69
5	47.00	$47.56^{\rm b}$	30.49	$30.62^{\rm b}$	24.52	24.72	21.33	21.44
10	59.61	$60.26^{\rm b}$	39.49	39.88	32.31	32.48	28.22	28.32
20	75.50	$76.22^{\rm b}$	51.26	51.60	42.24	42.39	37.06	37.14
50	102.41	103.11	71.38	71.70	59.42	59.54	52.44	52.52
100	127.93	128.64	90.74	91.08	76.13	76.25	67.52	67.59
200	158.50	159.24	114.45	114.70	96.66	96.77	86.14	86.20
500	207.47	208.52	153.17	153.43	130.62	130.76	117.15	117.24
1000	252.30	253.21	188.72	189.18	162.17	162.42	146.17	146.34

^aMulti-configurational Hartree-Fock method (Ruder et al. 1994)

Note. — All energies are in eV. $\Delta \tilde{z} = 2 \times 10^{-2}$.

 $^{^{\}mathrm{b}}\mathrm{Energies}$ are calculated by the spherical expansion of wave functions.

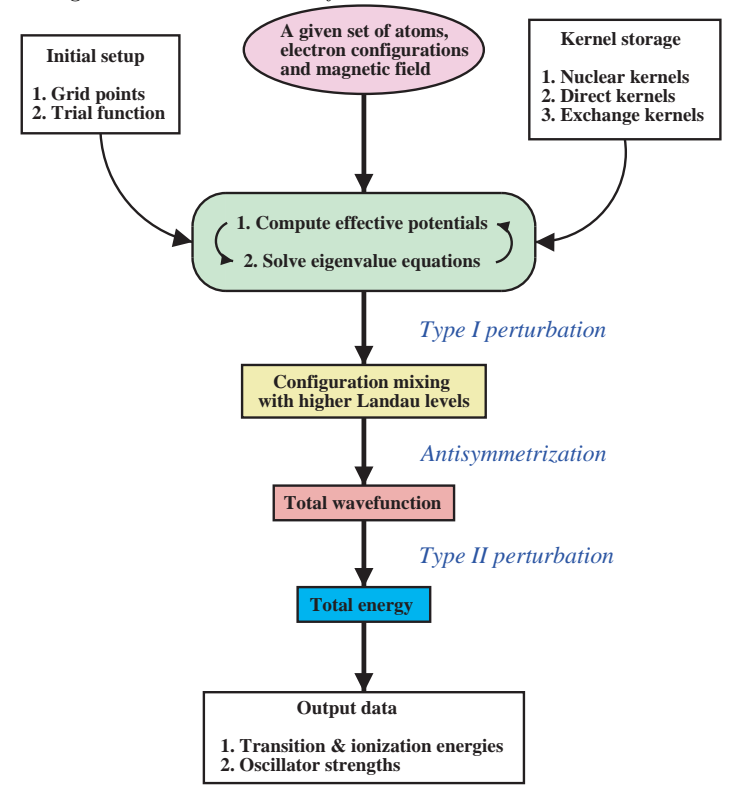


Fig. 3.— Algorithm of the Multi-configurational Perturbative Hybrid Hartree Hartree-Fock method.

Fig. 4.— Convergence test for the single-orbital Hartree energy of the innermost orbital $(m, \nu) = (0, 0)$ for Z = 2, 6, 14, 26 neutral atoms. $B_{12} = 1$, $\Delta \tilde{z} = 4 \times 10^{-2}$. All the electrons are in tightly-bound orbitals. There was minor change in the convergence speed for different magnetic fields and electron configurations.

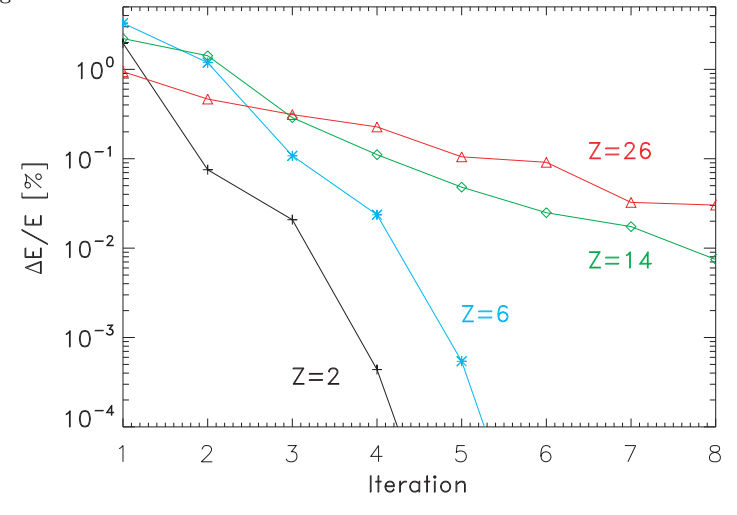


	Table	2		
Energies of	LOOSELY-BOUND	STATES	FOR	HYDROGEN.

(m, ν)	(0,1)		(0,2)		(1,1)		(1,2)	
β	Present work	$\mathrm{Ruder}^{\mathrm{a}}$	Present work	Ruder	Present work	Ruder	Present work	Ruder
1	8.051	$8.101^{\rm b}$	4.584	$4.733^{\rm b}$	6.653	6.673	3.832	3.876
2	9.096	$9.135^{\rm b}$	5.053	$5.138^{\rm b}$	7.759	7.778	4.314	4.346
5	10.38	10.41	5.650	5.684	9.221	9.224	4.940	4.961
10	11.24	11.24	6.076	6.090	10.23	10.23	5.396	5.411
20	11.94	11.94	6.480	6.481	11.10	11.12	5.834	5.845
50	12.62	12.62	6.956	6.971	12.05	12.05	6.381	6.388
100	12.96	12.96	7.310	7.319	12.55	12.56	6.767	6.775
200	13.20	13.20	7.632	7.647	12.94	12.94	7.136	7.140
500	13.39	13.40	8.040	8.051	13.24	13.25	7.590	7.590
1000	13.49	13.49	8.329	8.333	13.39	13.39	7.907	7.906

 $^{^{\}rm a}{\rm Multi\text{-}configurational~Hartree\text{-}Fock~method}$ (Ruder et al. 1994)

Note. — All energies are in eV. $\Delta z = 0.2$.

 $\begin{tabular}{ll} Table 3 \\ Ground state energies for helium. \\ \end{tabular}$

β_z	Present work	Ruder ^a	Jones ^b
1 2 5 10 20 50 100 200	146.06 (134.36) 184.73 (176.34) 255.39 (249.71) 326.05 (322.31) 414.92 (412.19) 564.50 (562.74) 707.15 (705.91) 880.00 (879.14)	134.29 176.30 249.80 322.22 412.26 563.61 706.99 879.04	146.94 186.85 258.19 329.27 418.22 568.39 710.95
500	$1158.49\ (1158.49)$	1156.63	
1000	1410.90 (1410.90)	1409.13	

^a1DHF (Ruder et al. 1994)

Note. — All energies are in eV. The ground state configuration is $(m,\nu)=(0,0),(1,0)$. $\beta_Z=1$ for helium corresponds to 1.88×10^{10} G. Bracketed values are results from our single-configurational calculation. $\Delta \tilde{z}=4\times 10^{-2}$. $N_{iter}=3$.

^bEnergies are calculated by the spherical expansion of wave functions.

^bUHF (Jones et al. 1999b)

 $\label{eq:table 4} \text{Table 4}$ Energies of excited states for helium at $\beta_Z=50.$

(m, ν)	Present work	Millera	Ruder ^b	Jones ^c
$ \begin{array}{c} (0,1) \\ (0,2) \\ (1,1) \\ (1,2) \\ (2,0) \\ (2,1) \end{array} $	423.29 418.34 421.72 416.61 521.73 421.45	413.7 408.8 412.2 407.8	421.71 416.17 419.68 415.25 521.37 419.49	426.39 420.88 424.38 419.95 525.97 424.18
(2,2)	416.26		414.83	419.52

^a1DHF (Miller & Neuhauser 1991)

^b1DHF (Ruder et al. 1994)

^cUHF (Jones et al. 1999b)

Note. — All energies are in eV. One electron is in $(m,\nu)=(0,0).$ $\Delta \tilde{z}=4\times 10^{-2}.$ $N_{iter}=3.$

 $\label{eq:table 5} \text{Ground state energies of neutral atoms through } Z = 1 - 14.$

		$B_{12} = 0.1$		B_{12}	= 0.5	
Z	Present work	Ivanov ^a	Neuhauser ^b	Present work	Ivanov	Neuhauser
1	0.0770 (0.0762)	0.07781	0.0761	0.1301 (0.1298)	0.13114	0.130
2	$0.2613\ (0.2557)$	0.26387	0.255	$0.4567 \ (0.4543)$	0.46063	0.454
3	0.5337(0.5160)	0.54042	0.516	$0.9526 \ (0.9449)$	0.96180	0.944
4	0.8897(0.8468)	0.89833	0.846	1.600 (1.580)	1.61624	1.580
5	1.327 (1.238)	1.33229	1.238	2.390 (2.349)	2.41101	2.347
6	1.854(1.687)	1.83895	1.678	3.308 (3.237)	3.33639	3.22
7	(2.186)	2.41607	2.17	4.353 (4.239)	4.38483	4.22
8	(2.754 [1])	3.08253[1]	2.71	5.517 (5.338)	5.55032	5.32
9	(3.377 [1])	3.82966 [1]	3.36	6.803 (6.544)	6.82794	6.51
10	(4.049 [1])	4.65087 [1]		8.198 (7.834)	8.21365	7.819
11	•••			9.718 (9.224)		9.197
12	• • •			11.410 [1] (10.750 [1])		10.72[1]
13	• • •			13.251 [1] (12.364 [1])		12.32 [1]
14		• • •	• • •	$15.246 \ [2] \ (14.062 \ [2])$		14.00 [1]

^a2DHF (Ivanov & Schmelcher 2000)

^b1DHF (Neuhauser et al. 1986)

Note. — All energies are in keV. The values in parentheses are single-configurational energy values. The number of $\nu=1$ orbitals are in square brackets (No brackets indicate all the electrons are in $\nu=0$ orbital). $\Delta \tilde{z}=(2-5)\times 10^{-2}$. $N_{iter}=5$.

 $\label{eq:Table 6} \mbox{Table 6}$ Ground state energies of neutral atoms through Z=1-26.

$B_{12} = 1.0$					$B_{12} = 5.0$			
Z	Present work	$Ivanov^a$	$\rm Neuhauser^b$	$\rm Jones^c$	Present work	Ivanov	Neuhauser	Jones
1	0.1614	0.16222	0.161		0.2558	0.25750	0.255	
2	0.5766	0.57999	0.574		0.9574	0.96191	0.958	1.040
3	1.214	1.22443	1.209		2.078	2.08931	2.076	
4	2.056	2.07309	2.042		3.586	3.61033	3.584	
5	3.085	3.10924	3.054		5.476	5.49950	5.456	
6	4.288	4.31991	4.20		7.695	7.73528	7.60	8.03
7	5.657	5.69465	5.54		10.231	10.29919	10.20	
8	7.176	7.22492	7.02		13.099	13.17543	13.00	
9	8.845	8.90360	8.63		16.264	16.34997	16.10	
10	10.664	10.72452	10.39	10.70	19.702	19.81072	19.57	20.24
11	12.625		12.25		23.406		24.64	
12	14.745		14.23		27.436		27.17	
13	16.973 [1]		16.34[1]		31.675		31.35	
14	19.408 [1]		18.60 [1]	19.09	36.154		35.74	36.76
15	21.987[1]		20.95[1]		40.915		40.35	
16	24.718 [2]		23.43 [2]		45.881		45.22	
17	27.618 [2]		26.07 [2]		51.067		50.30	
18	30.766 [2]		28.82 [2]		56.530		55.95	
19	34.036 [2]				62.181			
20	37.500 [3]			35.48	68.031			68.37
21					74.184 [1]			
22					80.602 [1]			
23					87.263 [1]			
24					94.259 [1]			
25					101.25 [1]			
26	(55.410 [5])		55.10 [6]	56.01	108.64 [2]		106.09[2]	108.18

^a2DHF (Ivanov & Schmelcher 2000)

Note. — All energies are in keV. $\Delta \tilde{z}=(2-5)\times 10^{-2}$. $N_{iter}=5$. Other atomic models computed several ground state energies. (1) Thomas-Fermi-Dirac method (Skjervold & Ostgaard 1984): 4.14, 7.73 [keV] for Z=6 at $B_{12}=1.0,5.0$. 56.21, 105.89 [keV] for Z=26 at $B_{12}=1.0,5.0$. (2) Restricted variational method (Flowers et al. 1977): 0.545, 0.913 [keV] for Z=2 at $B_{12}=1.0,5.0$. 53.13, 101.7 [keV] for Z=26 at $B_{12}=1.0,5.0$. (3) Density functional method with correction (Kössl et al. 1988) provide lower energy value 110.4 [keV] for Z=26 at $B_{12}=5.0$.

 ${\it Table 7}$ Oscillator strengths of bound-bound transitions for hydrogen.

$(m,\nu) \to (m',\nu')$	$\beta = 5$	$\beta = 10$	$\beta = 50$	$\beta = 100$	$\beta = 500$
$(0,0) \to (1,0)$	0.115 (0.108)	$7.15 \times 10^{-2} \\ (6.88 \times 10^{-2})$	$\substack{2.29 \times 10^{-2} \\ (2.32 \times 10^{-2})}$	$1.46 \times 10^{-2} \\ (1.44 \times 10^{-2})$	$5.04 \times 10^{-3} $ (5.06×10^{-3})
$(0,0) \to (0,1)$	0.627 (0.615)	0.553 (0.560)	0.437 (0.414)	$0.364 \\ (0.351)$	0.228 (0.227)
$(0,0) \to (0,3)$	$\begin{array}{c} 5.28 \times 10^{-2} \\ (5.24 \times 10^{-2}) \end{array}$	$\substack{4.93 \times 10^{-2} \\ (4.94 \times 10^{-2})}$	$\substack{4.19 \times 10^{-2} \\ (3.99 \times 10^{-2})}$	$\begin{array}{c} 3.64 \times 10^{-2} \\ (3.52 \times 10^{-2}) \end{array}$	$\substack{2.47 \times 10^{-3} \\ (2.45 \times 10^{-3})}$
$(1,0) \to (2,0)$	$\begin{array}{c} 8.80 \times 10^{-2} \\ (8.46 \times 10^{-2}) \end{array}$	$5.47 \times 10^{-2} \\ (5.47 \times 10^{-2})$	$1.97 \times 10^{-2} \\ (1.98 \times 10^{-2})$	$1.30 \times 10^{-2} \\ (1.30 \times 10^{-2})$	$5.47 \times 10^{-3} $ (5.48×10^{-3})
$(0,1) \to (0,2)$	1.53 (1.52)	1.50 (1.48)	1.38 (1.38)	1.33 (1.33)	1.20 (1.20)

Note. — Grid points are the same as in the tables of energy values. The values in parentheses are from multi-configurational Hartree-Fock method (Ruder et al. 1994). For $\Delta m=1$ transitions, finite nuclear mass correction is included.

 $^{^{\}rm b}1{
m DHF}$ (Neuhauser et al. 1986)

^cDF (Jones 1985b)

			Table 8			
OSCILLATOR	STRENGTHS	OF	BOUND-BOUND	TRANSITIONS	FOR	HELIUM.

(m, ν)	$\beta_Z = 5$	$\beta_Z = 10$	$\beta_Z = 50$	$\beta_Z = 100$	$\beta_Z = 500$
$(1,0) \to (1,1)$	0.523 (0.500)	0.424 (0.410)	$0.240 \\ (0.239)$	0.187 (0.184)	0.103 (0.099)
$(1,0) \to (2,0)$	$7.52 \times 10^{-2} \\ (7.35 \times 10^{-2})$	$\substack{4.56 \times 10^{-2} \\ (4.64 \times 10^{-2})}$	$1.51 \times 10^{-2} \\ (1.54 \times 10^{-2})$	$\begin{array}{c} 9.27 \times 10^{-3} \\ (9.36 \times 10^{-3}) \end{array}$	$\substack{2.85 \times 10^{-3} \\ (2.85 \times 10^{-3})}$
$(2,0) \to (2,1)$	$0.609 \\ (0.598)$	$0.522 \\ (0.511)$	$0.335 \\ (0.318)$	$0.253 \\ (0.250)$	0.133
$(2,0) \to (3,0)$	$\substack{4.45\times10^{-2}\\(4.50\times10^{-2})}$	$\substack{2.86 \times 10^{-2} \\ (2.87 \times 10^{-2})}$	$\begin{array}{c} 9.69 \times 10^{-3} \\ (9.74 \times 10^{-3}) \end{array}$	$\substack{6.00\times10^{-3}\\(6.02\times10^{-3})}$	$\substack{1.90 \times 10^{-3} \\ (1.90 \times 10^{-3})}$
$(3,0) \to (3,1)$	$0.663 \\ (0.661)$	$0.582 \\ (0.577)$	$0.380 \\ (0.375)$	$0.308 \\ (0.299)$	0.145

Note. — Grid points are the same as in the tables of energy values. The values in parentheses are from 1DHF (Ruder et al. 1994).

 $\label{eq:table 9} \text{Oscillator strengths of bound-bound transition } (m,0) \to (m,1) \text{ for carbon.}$

\overline{m}	$\beta = 200$	$\beta = 500$	$\beta = 1000$
0	$\substack{4.10 \times 10^{-2} \\ (3.97 \times 10^{-2})}$	$1.30 \times 10^{-2} \\ (1.11 \times 10^{-2})$	$5.81 \times 10^{-3} $ (5.71×10^{-3})
1	$\begin{array}{c} 5.98 \times 10^{-2} \\ (5.67 \times 10^{-2}) \end{array}$	$\substack{2.25\times 10^{-2}\\ (2.31\times 10^{-2})}$	$1.28 \times 10^{-2} \\ (1.35 \times 10^{-2})$
2	$7.97 \times 10^{-2} \\ (8.00 \times 10^{-2})$	$\substack{3.92 \times 10^{-2} \\ (3.80 \times 10^{-2})}$	$\substack{2.47 \times 10^{-2} \\ (2.36 \times 10^{-2})}$
3	0.114 (0.109)	$\substack{6.11 \times 10^{-2} \\ (5.65 \times 10^{-2})}$	$\begin{array}{c} 3.77 \times 10^{-2} \\ (3.62 \times 10^{-2}) \end{array}$
4	0.156 (0.144)	$\begin{array}{c} 8.63 \times 10^{-2} \\ (7.94 \times 10^{-2}) \end{array}$	$5.72 \times 10^{-2} $ (5.21×10^{-2})
5	0.197 (0.193)	0.116 (0.113)	$7.83 \times 10^{-2} \\ (7.55 \times 10^{-2})$

Note. — The values in parentheses are from 1DHF (Miller 1990). The other electrons are in their ground state.